COMMUNICATIONS IN COMPUTATIONAL PHYSICS
Vol. **2**, No. 6, pp. 1055-1070

Commun. Comput. Phys.
December 2007

Lattice Poisson-Boltzmann Simulations of Electroosmotic Flows in Charged Anisotropic Porous Media

Moran Wang[1,2,*], Ning Pan[1], Jinku Wang[3] and Shiyi Chen[2,4]

[1] *Department of Biological & Agricultural Engineering, University of California, Davis, CA 95616, USA.*
[2] *Department of Mechanical Engineering, Johns Hopkins University, Baltimore, MD 21218, USA.*
[3] *School of Aerospace, Tsinghua University, Beijing, China.*
[4] *College of Engineering, Peking University, Beijing, China.*

Received 7 November 2006; Accepted (in revised version) 7 March 2007

Available online 15 June 2007

Abstract. This paper presents numerical analysis of electroosmotic flows (EOF) in charged anisotropic porous media using the lattice Poisson-Boltzmann method (LPBM), which combines two sets of lattice evolution methods solving the nonlinear Poisson equation for electric potential distribution and the Navier-Stokes equations for fluid flow respectively. Consistent boundary condition implementations are proposed for solving both the electrodynamics and the hydrodynamics on a same grid set. The anisotropic structure effects on EOF characteristics are therefore studied by modeling the electrically driven flows through ellipse arrays packed in a microchannel whose shape and orientation angle are used to control the anisotropy of porous media. The results show that flow rates increase with the axis length along the external electric field direction for a certain porosity and decrease with the angle between the semimajor axis and the bulk flow direction when the orientation angle is smaller than $\pi/2$. After introducing random factors into the microstructures of porous media, the statistical results of flow rate show that the anisotropy of microstructure decreases the permeability of EOFs in porous media.

PACS (2006): 47.56.+r; 47.57.jd

Key words: Electroosmotic flow, anisotropic porous media, lattice Poisson-Boltzmann method.

1 Introduction

Electroosmotic flows (EOF) in porous media have been studied for nearly two hundred years due to their important applications in soil, petroleum and chemical engineering

*Corresponding author. *Email addresses:* mmwang@ucdavis.edu (M. R. Wang), npan@ucdavis.edu (N. Pan), wjk01@mails.tsinghua.edu.cn (J. K. Wang), syc@jhu.edu (S. Y. Chen)

since the electrokinetic effects were first observed by Reuss in 1809 in an experimental investigation on porous clay [1-3]. In the past few decades, there are considerable and reawakening interests in the EOF in porous media because of the conspicuous applications in biological-chemical-medical analysis [4-6] and new techniques in energy and geophysical engineering [7,8], especially in micro- and nanoscales. Recently, charged porous structures have been employed in some devices to control and improve the fluid behavior as expected. Microparticles which are packed in microchannels have been used to improve the performances of electroosmotic micropumps with a lower flow rate and a higher pumping pressure [9-11]. Owing to the polarization effect of porous electrodes, the structured electrode arrays have been designed as a concentration demixer of electrolytes [12].

The EOF dynamics in porous media has been studied much both theoretically [13-20] and numerically [20-29]. By improving the simple capillary tube model [13], Mehta and Morse [14] schematized a micro porous membrane by an array of charged uniform spheres. Jin and Sharma [16] extended the capillary model to two-dimensional square lattice network model, which is more appropriate in simulating inhomogeneous porous media. Grimes et al. [18] developed the cubic lattice network of interconnected cylindrical pores model and simulated the intraparticle electroosmotic volumetric flow rate and velocity in the three-dimensional pore network of interconnected cylindrical pores. Generally, the theoretical models can give an overall prediction of the EOF characteristics, but few can present flow structure details. Besides the various theoretical models, pure numerical methods have been developed in the past decade for predicting details of EOF in porous media owing to the rapid developments of computer and computational techniques [20-28]. The premier efforts of the numerical predictions for the EOF in porous media focused on the linearized model of nonlinear governing equation for electric potential distribution due to the numerical instability and time-consuming characteristic of solving the original nonlinear Poisson-Boltzmann equation [20-25]. However, both experimental data and the first principle analysis have indicated that when the zeta potential is greater than 30 mV the linear assumption of the Poisson-Boltzmann equation will break down [29,30].

Hlushkou et al. [26] proposed a numerical scheme for modeling the EOF in porous media, which involves a traditional finite-difference method (FDM) for solving the nonlinear Poisson-Nernst-Planck equations for electrodynamics and a lattice Boltzmann method (LBM) for Navier-Stokes equations for hydrodynamics. The coupled methods have been used to investigate the flow fields between random arrays of spheres [27] and in colloids systems [28]. Almost at the same time, Wang et al. [31,32] presented a lattice Poisson-Boltzmann method (LPBM) for predicting the EOF in microchannels, which combines a lattice Poisson method (LPM) for solving the nonlinear Poisson equation for electric potential distribution with a lattice Boltzmann method (LBM) for solving the Boltzmann-BGK equations for fluid flow. The LPBM has been employed to analyze the mixing enhancement by EOF in microchannels [33] and the improved pumping performances by the changed isotropic porous media additives in micropumps [34]. To our

knowledge, no contributions have reported for full numerical analysis of the anisotropic porous media effects on the EOF.

Another interest is now focusing on the boundary condition treatment employed in the lattice Boltzmann method. We have noticed that the conventional bounce-back model was used in both Hlushkou's coupling method [26-28] and the early research of Wang's LPBM [31]. The bounce-back model succeeds in dealing with complicated boundary geometries with easy implementations [35,36], however suffers from its non-physical significance at the same time [37-39]. For a boundary, flat or curve, implemented by the bounce-back rule, the physical non-slip fluid boundary is not located on the boundary nodes, but on somewhere between the boundary nodes and the nodes next to them [40]. That is to say the LBM with a bounce-back rule for boundary conditions may be inconsistent with other partial differential equations (PDE) solvers on the same grid set.

The objective of the present contribution is to present numerical modeling results of the EOF through charged anisotropic porous media using the lattice Poisson-Boltzmann method. The boundary condition implementations are studied and treated correctly to insure consistent for the different PDE solvers on one grid set. The anisotropic porous media are represented by a series of ellipses arrays, of which the axis lengths and the orientation angle can be used to control the media anisotropy. The directional characteristics of the EOF in anisotropic porous media arrays are mainly concerned. The ellipse arrays with random axis lengths and random angles are also studied.

2 Numerical method

2.1 Governing equations

When the polarization and chemical absorption effects are negligible, the velocity filed of an incompressible Newtonian fluid is governed by the Navier-Stokes equation [3,27,41]. The flow velocity $\mathbf{u}$ of the electrolyte solution representing a divergence-free velocity filed ($\nabla\cdot\mathbf{u}=0$) is given by

$$\rho\frac{\partial\mathbf{u}}{\partial t}+\rho\mathbf{u}\cdot\nabla\mathbf{u}=-\nabla P+\mu\nabla^2\mathbf{u}+\rho_e\mathbf{E}, \tag{2.1}$$

where P is the hydrostatic pressure, ρ and μ are the mass density and the dynamic viscosity of fluid, respectively, ρ_e the net charge density, and $\mathbf{E}$ the external electric field strength. The Navier-Stokes equation could be simplified as Stokes equation for very low-Reynolds flows.

Electric double layer (EDL) theory [42] relates the electrostatic potential and the distribution of counter-ions and co-ions in the bulk solution by the Poisson equation

$$\nabla^2\psi=-\frac{\rho_e}{\varepsilon\varepsilon_0}, \tag{2.2}$$

where ψ is the electrical potential, ε the dimensionless dielectric constant of the solution, and ε_0 the permittivity of a vacuum. The ionic migration is governed by the Nernst-

Plank equation in general; however this process can be simplified due to very low flow speed in microfluidics [3]. According to classical EDL theory, the equilibrium Boltzmann distribution equation can be used to describe the ionic number concentration. Therefore, the net charge density distribution can be expressed as the sum of all the ions in the solution

$$\rho_e = \sum_i z_i e n_{i,\infty} \exp\left(-\frac{z_i e}{k_b T}\psi\right), \tag{2.3}$$

where the subscript i represents the ith species, n_∞ is the bulk ionic number concentration, z the valence of the ions (including the sign), e the absolute value of one proton charge, k_b the Boltzmann constant, and T the absolute temperature. In the present work, we considered only binary electrolyte, but our method can deal more than binary electrolyte solutions.

Substituting Eq. (2.3) into Eq. (2.2) yields the nonlinear Poisson-Boltzmann equation for the electrical potential in the dilute electrolyte solution

$$\nabla^2\psi = -\frac{1}{\varepsilon\varepsilon_0}\sum_i z_i e n_{i,\infty} \exp\left(-\frac{z_i e}{k_b T}\psi\right). \tag{2.4}$$

Associated with the governing equations, the Dirichlet type of boundary condition is used to describe the solid-fluid interface for either the electrodynamics or the hydrodynamics. Both a non-slip boundary condition with zero normal flux and the surface zeta potential are specified on the solid surface, which have been proved for most cases by atomistic simulations as long as the channel size is much larger than 10 molecular diameters, especially for dilute solutions [43-45].

2.2 Lattice Poisson-Boltzmann method

The electric potential and velocity fields of the EOF can be solved using the lattice Poisson-Boltzmann method (LPBM) proposed by our previous work [31,32], which combines a evolution method for electric potential on discrete lattices to solve the nonlinear Poisson equation (Lattice Poisson method) with a evolution method for density on discrete lattices to solve the Boltzmann-BGK equation (Lattice Boltzmann method).

For a two-dimensional case, the discrete nine-speed lattice evolution equation to solve the hydrodynamic equations can be written as [46-48]

$$f_\alpha(\mathbf{r}+\mathbf{e}_\alpha\delta_t, t+\delta_t) - f_\alpha(\mathbf{r},t) = -\frac{1}{\tau_\nu}\left[f_\alpha(\mathbf{r},t) - f_\alpha^{eq}(\mathbf{r},t)\right] + \delta_t F_\alpha, \tag{2.5}$$

where $\mathbf{r}$ is the position vector, δ the time step, $\mathbf{e}_\alpha$ the discrete velocity

$$\mathbf{e}_\alpha = \begin{cases} (0,0), & \alpha = 0, \\ (\cos\theta_\alpha, \sin\theta_\alpha)c, & \theta_\alpha = (\alpha-1)\pi/2, \quad \alpha = 1,2,3,4, \\ \sqrt{2}(\cos\theta_\alpha, \sin\theta_\alpha)c, & \theta_\alpha = (\alpha-5)\pi/2+\pi/4, \quad \alpha = 5,6,7,8, \end{cases} \tag{2.6}$$

where c is the sound speed, τ_ν the dimensionless relaxation time which is a function of the fluid viscosity

$$\tau_\nu = 3\nu\frac{\delta_t}{\delta_x^2}+0.5, \tag{2.7}$$

where ν is the kinetic viscosity and δ_x the lattice constant. The density equilibrium distribution is then

$$f_\alpha^{eq} = \omega_\alpha \rho_0 \left[1+3\frac{\mathbf{e}_\alpha\cdot\mathbf{u}}{c^2}+9\frac{(\mathbf{e}_\alpha\cdot\mathbf{u})^2}{c^4}-\frac{3\mathbf{u}^2}{2c^2}\right], \tag{2.8}$$

with

$$\omega_\alpha = \begin{cases} 4/9, & \alpha=0, \\ 1/9, & \alpha=1,2,3,4, \\ 1/36, & \alpha=5,6,7,8. \end{cases} \tag{2.9}$$

The external force term F_α in Eq. (2.5) should include both the pressure and the electric force effects [31,32]

$$F_\alpha = \frac{(-\nabla P+\rho_e\mathbf{E}-\rho_e\nabla\Phi)\cdot(\mathbf{e}_\alpha-\mathbf{u})}{\rho RT} f_\alpha^{eq}, \tag{2.10}$$

where Φ is the stream electrical potential caused by the ion movements in the solution based on the Nernst-Planck theory.

The macroscopic density and velocity can be calculated using

$$\rho = \sum_\alpha f_\alpha, \tag{2.11}$$

$$\rho\mathbf{u} = \sum_\alpha e_\alpha f_\alpha. \tag{2.12}$$

Borrowing the spirit from the Lattice Boltzmann method, Eq. (2.4) is re-written by expanding a time-dependent term

$$\frac{\partial\psi}{\partial t} = \nabla^2\psi + g_{rhs}(\mathbf{r},\psi,t), \tag{2.13}$$

where

$$g_{rhs} = \frac{1}{\varepsilon\varepsilon_0}\sum_i z_i e n_{i,\infty}\exp\left(-\frac{z_i e}{k_b T}\psi\right) \tag{2.14}$$

represents the negative right hand side (RHS) term of the original Poisson-Boltzmann equation. The solution of Eq. (2.4) is the steady solution of Eq. (2.13). The evolution equation for the electrical potential on the two-dimensional discrete lattices can then be written as [31,49]

$$g_\alpha(\mathbf{r}+\Delta\mathbf{r},t+\delta_{t,g})-g_\alpha(\mathbf{r},t) = -\frac{1}{\tau_g}\left[g_\alpha(\mathbf{r},t)-g_\alpha^{eq}(\mathbf{r},t)\right]+\left(1-\frac{0.5}{\tau_g}\right)\delta_{t,g}\omega_\alpha g_{rhs}, \tag{2.15}$$

where

$$g_\alpha^{eq}=\omega_\alpha\psi,\quad \text{with}\quad \omega_\alpha=\begin{cases}0, & \alpha=0,\\ 1/6, & \alpha=1,2,3,4,\\ 1/12, & \alpha=5,6,7,8,\end{cases} \tag{2.16}$$

and the time step is

$$\delta_{t,g}=\frac{\delta_x}{c'}, \tag{2.17}$$

where c' is a pseudo sound speed in the potential field. The dimensionless relaxation time is

$$\tau_g=\frac{3\delta_{t,g}}{2\delta_x^2}+0.5. \tag{2.18}$$

After evolving on the discrete lattices, the macroscopic electrical potential can be calculated using

$$\psi=\sum_\alpha(g_\alpha+0.5\delta_{t,g}g_{rhs}\omega_\alpha). \tag{2.19}$$

2.3 Boundary conditions

The boundary condition implementations play a very critical role to the accuracy of the numerical simulations. The hydrodynamic boundary conditions for the lattice Boltzmann method have been studied extensively [37-40, 50-53]. The conventional bounce-back rule is the most commonly used method to treat the velocity boundary condition at the solid-fluid interface due to its easy implementation, where momentum from an incoming fluid particle is bounced back in the opposite direction as it hits the wall [46]. However the conventional bounce-back rule has two main disadvantages. First, it requires the dimensionless relaxation time strictly within the range of (0.5, 2), otherwise the prediction will deviate from the correct result definitely [37,38]. Second, the non-slip boundary implemented by the conventional bounce-back rule is not located on the boundary nodes exactly, as mentioned before, which will lead to inconsistence when coupling with other PDE solvers on a same grid set [40].

To overcome the inconsistence between the LBM and other PDE solvers on a same grid set, one can replace the bounce-back rule with another "non-slip" boundary treatment proposed by Inamuro et al. [50], of course with the cost of loss of easy implementation for complicated geometries. An alternative solution is to modify the boundary condition treatments of the PDE solver for the electric potential distribution to be consistent with the LBM bounded by the bounce-back rule. In this contribution, the half-way bounce-back rule [51,40] for nonequilibrium distribution proposed by Zou and He [39] is introduced and extended to both hydrodynamic and electrodynamic boundary implementations to deal with the complex geometries in porous media.

At the boundary the following hydrodynamic boundary condition holds:

$$f_\alpha^{neq}=f_\beta^{neq}, \tag{2.20}$$

where α and β represent two opposite directions. Analogously, the nonequilibrium "bounce-back" rule for the electric potential distribution function at wall surfaces is suggested as:

$$g_{\alpha}^{neq} = -g_{\beta}^{neq}. \tag{2.21}$$

The "half-way" bounce-back scheme with interpolation is used here to deal with the curved surfaces in porous media [52,53]. This boundary treatment has a super-linear accuracy when the wall surface varies between two nodes and an approximately second-order accuracy if the wall surface locates at the middle [39,40]. This method is easy for complicated boundary condition implementations without any additional considerations. Periodic conditions were implemented at the inlet and the outlet.

3 Results and discussion

Before the LPBM is applied to simulate the EOF in anisotropic porous media, the boundary treatment effects on the velocity field results are examined. The failure reasons of the previous works will be analyzed based on the results. The present numerical method associated with the consistent boundary treatment methods is then employed to simulate and analyze the anisotropy influences of the microstructure of charged ellipse arrays on the transport characteristics of the EOF. Finally, the random factors are introduced into the porous structure and the effects on the EOF are therefore analyzed.

3.1 Boundary treatment effects

As stated before, the solid-fluid interface boundary implemented by the conventional bounce-back rule of LBM is not really located at the boundary nodes but at somewhere between the boundary nodes and the nodes next to them. For a flat plate channel flow, the calculated non-slip boundaries are actually located at the middle between the boundary nodes and the inner nodes next to them. Fig. 1 shows the velocity profiles for a simple two-dimensional Poisseuille flow in a flat plate channel calculated by the LBM with the conventional bounce-back boundary treatment. The circle-line is the result plotted on the original grid which deviates the parabolic rule remarkably near the boundaries. When both the boundaries are moved into the fluid for a half lattice distance, the numerical results agree almost exactly with the theoretical solutions for the Poisseuille flow. The two vertical dashed lines are the actual boundary locations for the conventional bounce-back treatment for LBM. That is also to say if the lattice number in width is N, the real channel width is not $(N-1)\cdot\delta_x$ but $(N-2)\cdot\delta_x$ with δ_x representing the lattice constant.

No literature has reported that the finite deference method (FDM) has the same characteristics at the boundary as the conventional bounce-back treatment for LBM. Therefore there is a half lattice difference even though the FDM and the LBM are solved on the same grid set. A system error is thus introduced into the calculation of the electrical driven force on each node. The interpolations can reduce but can not totally remove the system

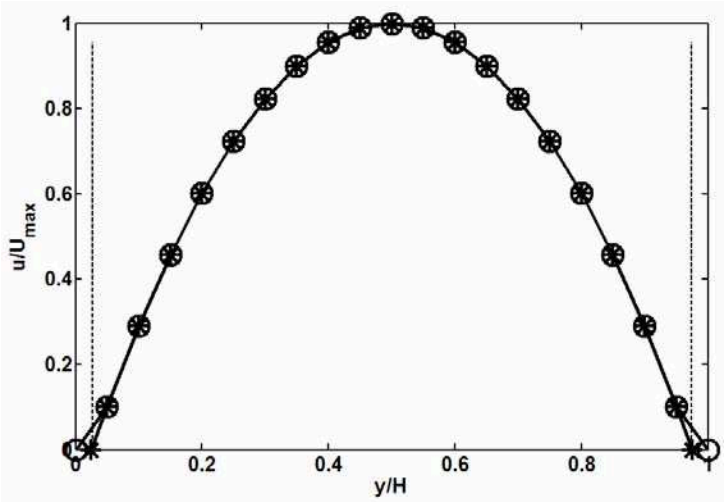

Figure 1: Velocity profiles by the LBM with the conventional bounce-back boundary treatment for a Poiseuille flow in a flat plate channel. The circle-line represents the results plotted on the original grid; the star-line represents the results plotted on the modified gird where the boundary locates at the half lattice position. The modified results agree exactly with the corresponding theoretical solutions.

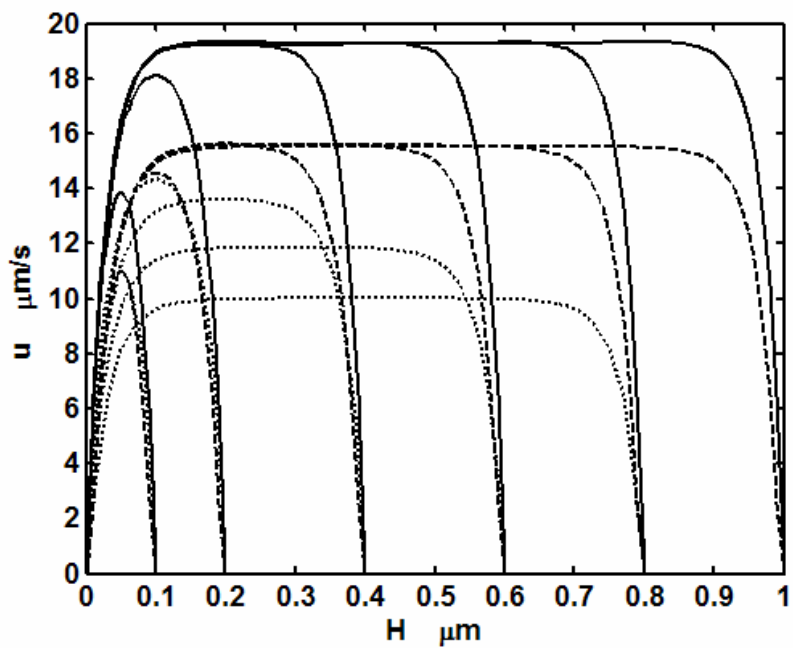

Figure 2: Velocity profiles of two-dimensional EOF in flat plate channels for different channel widths calculated using different methods and grids. The solid lines (—) represent the results using the present LPBM with consistent half-way boundary treatments and each lattice represents 0.01 micron; the dash-lines (- -) represent the results using the coupling FDM-LBM scheme [26-28] where the conventional bounce-back model is used for LBM and the grid is the same as the former one; the dotted lines (...) represent the results using the LPBM scheme with a conventional bounce-back model for LBM and the grid number keeps constant (40 in width) for each case [31].

error due to the strong boundary-layer-like distribution of the electric potential near the solid surface. The dash-lines in Fig. 2 are the velocity profiles of EOF in plate channels for different channel widths using the coupling FDM-LBM scheme [27]. Comparing with the results using the present LPBM with consistent boundary treatments (solid lines), the velocities results from the coupling FDM-LBM method are lower. For current coupling FDM-LBM simulations, the grid number are same as that in LPBM for each channel width and the lattice constant δ_x holds on a fine constant value, 0.01 μm. Therefore, the current FDM-LBM simulations give a similar qualitative result as the present LPBM simulations do. Because of the half lattice distance difference between the two methods in the coupling scheme, the calculated velocities of EOF are very sensitive to the lattice constant (grid size) for each simulation.

The dotted lines in Fig. 2 show the velocity profiles for different channel widths, where the grid number in width keeps constant at 40 for each case and the lattice constant therefore varies. The results indicate the calculated velocity of EOF by the coupling method with inconsistent boundary treatments decreases with the lattice constant. A similar result can be found in our previous work [31], which was also caused by the inconsistent boundary treatments for electrodynamics and for hydrodynamics. The correct results in Fig. 2 with modified boundary implementations also indicate that the flow rate increases monotonically with the flux area (channel width).

3.2 Anisotropic structure effects

Since the EOF though isotropic porous media has been investigated using the spheres arrays [27,34], the anisotropic structure effects on the EOF will be studied in this work by using the ellipses array where the axis lengths and the angle are used to control the anisotropy of the media.

Consider a two-dimensional steady-state isothermal EOF in a microchannel packed with an array of ellipses, as shown in Fig. 3(a). The channel walls are charged with zeta potential ζ_{wall}. The charged ellipses are nondeformable, impermeable, nonconducting and uniformly distributed in the microchannel with equal intervals between in both left-right and up-down directions. Every ellipse is assumed homogeneously charged at a same zeta potential $\zeta_{ellipse}$ with no polarization. The shape of each ellipse is determined by three parameters, a, b and θ, as shown in Fig. 3(b), where a and b are the length of the semimajor and the semiminor axes, respectively and θ is the orientation angle. The electrolyte solution can be driven by the external electric field, E, flowing through the anisotropic porous media structured by the ellipse array.

In the following simulations, we change the values of a, b and θ with remaining the porosity $\varepsilon = 0.33$. The other parameters are: the channel width $H = 1$ μm and 240×120 grid is used in our simulations; the surface charge zeta potential of both the channel walls and the ellipses $\zeta_{wall} = \zeta_{ellipse} = -50$ mV; the relative dielectric constant of the electrolyte solution $\varepsilon = 81$, the density $\rho = 1000$ kg/m^3 and the dynamic viscosity $\mu = 0.889$ mPa·s; the bulk ionic concentration of the solution $c_\infty = 10^{-4}$ M and the external electric field

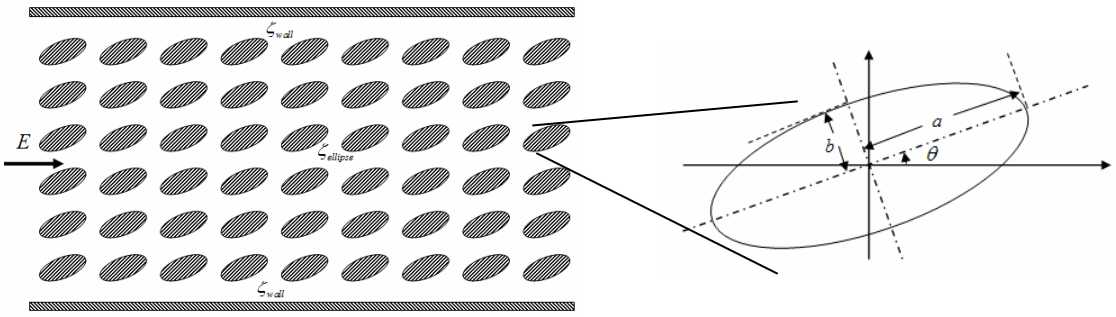

Figure 3: Schematic illustrations of the ellipse array packed in a microchannel and the microstructure of each ellipse.

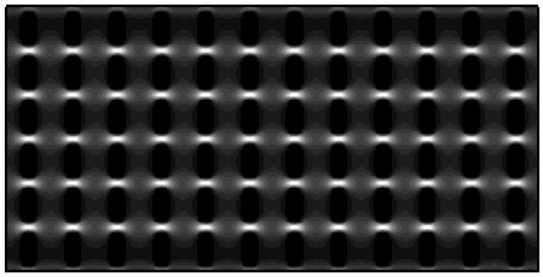

(a) $a=38.5$ nm, $b=64.9$ nm, $\theta=0$.

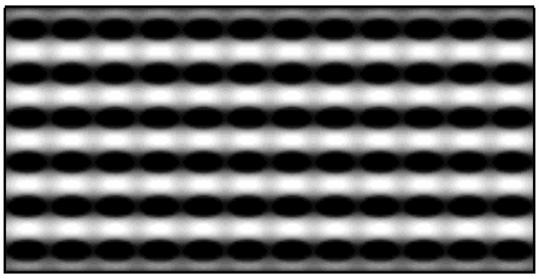

(b) $a=69.2$ nm, $b=36.1$ nm, $\theta=0$.

Figure 4: The x-velocity color contours for different axes lengths with zero orientation angle.

strength E=5 kV/m. a and b are independent for a certain porosity. To avoid blocking the flow, a changes from 34.6 to 79.2 nm. We set the relative error tolerance at 10^{-5} per 100 steps. Each calculation took a few hours on 2.0 G CPU depending on the simulation parameters.

Firstly, we change the value of the axis length in x direction, a, while keep the orientation angle θ at zero. With the value of a increasing, the anisotropy changes from y-dominating to x-dominating. As a result, the flow rate will increase with a because the external electric field is parallel to x-direction. Fig. 4 shows the contours of x-directional velocity for $a=38.5$ nm and $a=69.2$ nm respectively. The velocity and flux area for a

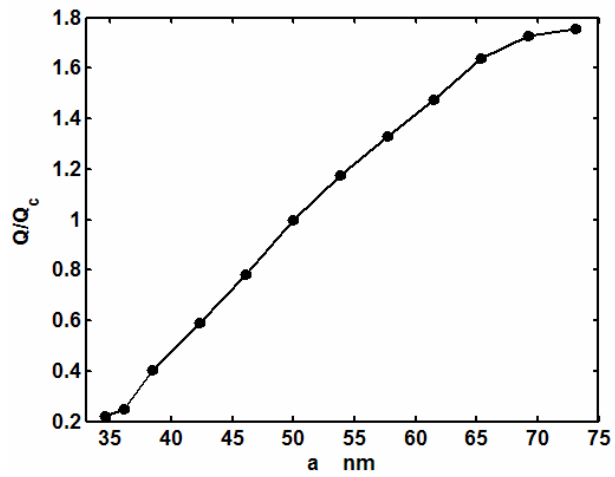

Figure 5: The flow rate versus the length of a when $\theta=0$. The flow rates are normalized by the case when the ellipse is a circle $a=b$.

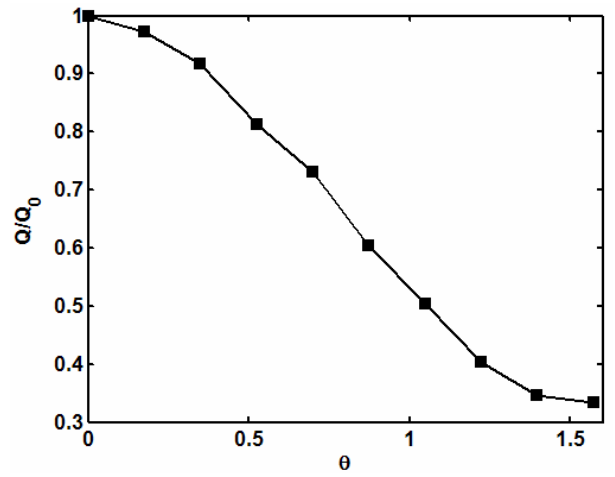

Figure 6: The flow rate versus the orientation angle θ when $a=61.5$ nm and $b=40.6$ nm. The flow rates are normalized by the case when $\theta=0$.

greater a are much larger than those for a lower a. However the flow rate is not dependent on the value of a at a rigorous proportional relationship, as shown in Fig. 5. The results show that when the axis length a is very small (<40 nm) or very large (>65 nm), the increasing speed of flow rate becomes much lower. The mechanism needs more investigations.

Secondly, we keep the axes lengths, a and b, invariable, but change the orientation angle θ. In the present work, we choose $a=61.5$ nm and $b=40.6$ nm. The orientation angle varies from 0 to $\pi/2$. Fig. 6 shows the calculated flow rate versus the orientation angle θ. The flow rate decreases with the orientation angle when the angle varies within

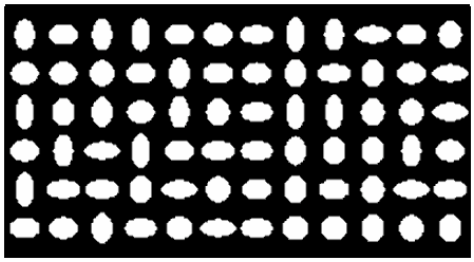

(a) random axes length at $\theta = 0$

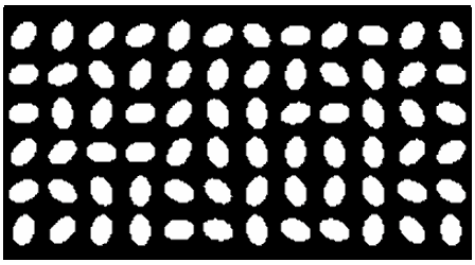

(b) random orientation angles at $a = 61.5$ nm, $b = 40.6$ nm

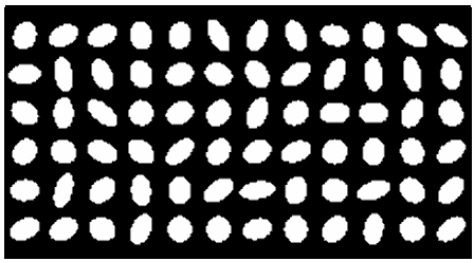

(c) random axes length and random orientation angles

Figure 7: Anisotropic porous media morphologies with random factors.

$(0, \pi/2)$. Considering the symmetry of the microstructure, the flow rate depends on the orientation angle with a near-cosine rule.

3.3 Random anisotropic media

Besides the structured anisotropic porous media above, the random factors have been introduced into the morphologies. In this contribution, we have focused on three aspects: i) randomly generated axes length at a fixed orientation angle; ii) randomly orientation angles with chosen axes length; iii) randomly generated axes length and orientation angles. Fig. 7 demonstrates the generated microstructure for each aspect respectively.

Since the random factors have been introduced during the generation of porous structures, the calculated effective thermal conductivity for the porous media with the statis-

tical characteristics will not be identical in every trial, but fluctuate around an average value. We performed 20 times of generations and calculations for each aspect in this work. The averaged flow rate for each case is $Q_i = 0.3235$ μl/min, $Q_{ii} = 0.3118$ μl/min, $Q_{iii} = 0.3061$ μl/min. The flow rate of the EOF in the isotropic porous media structured by sphere arrays is 0.4088 μl/min with same parameters and under same boundary conditions. These results show that the anisotropy of microstructure decreases the permeability of the EOF in porous media. The reason may be that the anisotropy decreases the average flux area.

4 Conclusions

Electroosmotic flow in charged anisotropic porous media has been numerically studied using the lattice Poisson-Boltzmann method. Consistent boundary condition implementations have been presented in this paper for solving both the electrodynamics and the hydrodynamics on a same grid set. The present method revises the half-grid difference between other different PDE solvers and the LBM associated with the conventional bounce-back rule near the boundary in previous works, and is suitable for modeling EOF in porous media with complicated morphologies.

Employing ellipse arrays packed in a microchannel whose shape and angle are used to control the anisotropy of porous media, the anisotropic structure effects on the EOF characteristics have been numerically studied. The results show that flow rates increase with the axis length along the external electric field direction for a certain porosity and decrease with the angle between the semimajor axis and the bulk flow direction when the angle is smaller than $\pi/2$. After introducing the random factors into the generations of microstructure of porous media, the statistical results of flow rate show that the anisotropy of microstructure decreases the permeability of the EOF in porous media.

Acknowledgments

The present work is supported by a grant from the NTC-M04-CD01 and NSF-061308 of USA and the NSF (59995550-2) of China.

References

[1] F. Reuss, Sur un nouvel effect de l'electricte galvanique, Memoires de la Societe Imperiale de Naturalistes de Moscou, 2 (1809), 327-337.
[2] K. P. Tikhomolova, Electro-osmosis, Ellis Horwood, New York, 1993.
[3] D. Q. Li, Electrokinetics in Microfluidics, Academic Press, Oxford, 2004.
[4] A. K. Banga, Electrically Assisted Transdermal and Topical Drug Delivery, Taylor & Francis Group, 1998.
[5] R. E. Oosterbroek and A. van den Berg, Lab-on-a-Chip: Miniaturized Systems for (Bio) Chemical Analysis and Synthesis, Elsevier, Boston, 2003.

[6] P. K. Wong, J. T. Wang, J. H. Deval and C. M. Ho, Electrokinetic in micro devices for biotechnology applications, IEEE/ASME T. Mechatronics, 9 (2004), 366-376.
[7] D. Beamish and R. J. Peart, Electrokinetic geophysics–a review, Terra Nova, 10(1) (1998), 48-55.
[8] C. Y. Wang, Fundamental models for fuel cell engineering, Chem. Rev., 104 (2004), 4727-4766.
[9] S. L. Zeng, C. H. Chen, J. C. Mikkelsen and J. G. Santiago, Fabrication and characterization of electroosmotic micropumps, Sensor. Actuat. B-Chem., 79(2-3) (2001), 107-114.
[10] S. H. Yao and J. G. Santiago, Porous glass electroosmotic pumps: theory, J. Colloid Interface Sci., 268(1) (2003), 133-142.
[11] J. A. Tripp, F. Svec, J. M. J. Frechet, S. L. Zeng, J. C. Mikkelsen and J. G. Santiago, High-pressure electroosmotic pumps based on porous polymer monoliths, Sensor. Actuat. B-Chem., 99(1) (2004), 66-73.
[12] F. C. Leinweber, J. C. T. Eijkel, J. G. Bomer and A. van den Berg, Continuous flow microfluidic demixing of electrolytes by induced charge electrokinetics in structured electrode arrays, Anal. Chem., 78 (2006), 1425-1434.
[13] L. Dresner, Electrokinetic phenomena in charged microcapillaries, J. Phys. Chem., 67(8) (1963), 1635.
[14] G. D. Mehta and T. F. Morse, Flow through charged membranes, J. Chem. Phys., 63(5) (1975), 1878-1889.
[15] M. W. Kozak and E. J. Davis, Electrokinetic phenomena in fibrous porous media, J. Colloid Interface Sci., 112(2) (1986), 403-411.
[16] M. Q. Jin and M. M. A. Sharma, Model for electrochemical and electrokinetic coupling in inhomogenerous porous media, J. Colloid. Interf. Sci., 142(1) (1991), 61-73.
[17] H. Ohshima, Electroosmotic velocity in fibrous porous media, J. Colloid. Interf. Sci., 210 (1999), 397-399.
[18] B. A. Grimes, J. J. Meyers and A. I. Liapis, Determination of the intraparticle electroosmotic volumetric flow-rate, velocity and Peclet number in capillary electrochromatography from pore network theory, J. Chromatogr. A, 890 (2000), 61-72.
[19] R. C. Wu and K. D. Papadopoulos, Electroosmotic flow through porous media: Cylindrical and annular models, Colloid. Surface. A, 161 (2000), 469-476.
[20] D. Coelho, M. Shapiro, J. F. Thovert and P. M. Adler, Electroosmotic phenomena in porous media, J. Colloid Interface Sci., 181(1) (1996), 169-190.
[21] S. Marino, D. Coelho, S. Békri and P. M. Adler, Electroosmotic phenomena in fractures, J, Colloid. Interf. Sci., 223 (2000), 292-304.
[22] S. Marino, M. Shapiro and P. M. Adler, Coupled transports in heterogeneous media, J. Colloid Interface Sci., 243(2) (2001), 391-419.
[23] M. R. Schure, R. E. Murphy, W. L. Klotz and W. Lau, High performance capillary gel electrochromatography with replaceable media, Anal. Chem., 70(23) (1998), 4985-4995.
[24] Y. J. Kang, C. Yang and X. Y. Huang, Analysis of the electroosmotic flow in microchannel packed with homogeneous microspheres under electrokinetic wall effect, Int. J. Eng. Sci., 42 (2004), 2011-227.
[25] M. Rosanne, M. Paszkuta and P. M. Adler, Electrokinetic phenomena in saturated compact clays, J. Colloid Interface Sci., 297 (2006), 353-364.
[26] D. Hlushkou, D. Kandhai and U. Tallarek, Coupled lattice-Boltzmann and finite-difference simulation of electroosmosis in microfluidic channels, Int. J. Numer. Meth. Fluid., 46(5) (2004), 507-532.
[27] D. Hlushkou, A. Seidel-Morgenstern and U. Tallarek, Numerical analysis of electroosmotic

flow in dense regular and random arrays of impermeable, nonconducting spheres, Langmuir, 21(13) (2005), 6097-6112.
[28] D. Hlushkou, V. Apanasovich, A. Seidel-Morgenstern and U. Tallarek, Numerical simulation of electrokinetic microfluidics in colloidal systems, Chem. Eng. Commun., 193(7) (2006), 826-839.
[29] M. J. Stevens and M. O. Robbins, Density functional theory of ionic screening: when do like charges attract, Europhys. Lett., 12(1) (1990), 81-86.
[30] R. J. Flatt and P. Bowen, Electrostatic repulsion between particles in cement suspensions: Domain of validity of linearized Poisson-Boltzmann equation for nonideal electrolytes, Cement Concrete Res., 33(6) (2003), 781-791.
[31] J. K. Wang, M. Wang and Z. X. Li, Lattice Poisson-Boltzmann simulations of electro-osmotic flows in microchannels, J. Colloid Interface Sci., 296(2) (2006), 729-736.
[32] M. Wang, J. K. Wang and Z. X. Li, Corrigendum to "Lattice Poisson-Boltzmann simulations of electro-osmotic flows in microchannels" [J. Colloid Interface Sci. 296 (2006) 729736], J. Colloid Interface Sci., 300(1) (2006), 446-446.
[33] J. K. Wang, M. Wang and Z. X. Li, Lattice Boltzmann simulations of mixing enhancement by the electro-osmotic flow in microchannels, Mod. Phys. Lett. B, 19(28-29) SI (2005), 1515-1518.
[34] M. Wang, J. K. Wang, S. Y. Chen and N. Pan, Electrokinetic pumping effects of charged porous media in microchannels using the lattice Poisson-Boltzmann method, J. Colloid Interface Sci., 304(1) (2006), 246-253.
[35] Q. J. Kang, D. X. Zhang, P. C. Lichtner and I. N. Tsimpanogiannis, Lattice Boltzmann model for crystal growth from supersaturated solution, Geophys. Res. Lett., 31 (2004), L21604.
[36] D. Raabe, Overview of the lattice Boltzmann method for nano- and microscale flow dynamics in materials science and engineering, Model. Simul. Mater. Sci. Eng., 12 (2004), R13-R46.
[37] D. R. Noble, S. Y. Chen, J. G. Georgiadis and R. O. Buckius, A consistent hydrodynamic boundary condition for the lattice Boltzmann method, Phys. Fluids, 7 (1995), 203-209.
[38] S. Y. Chen, D. Martinez and R. W. Ren, On boundary conditions in lattice Boltzmann methods, Phys. Fluids, 8 (1996), 2527-2536.
[39] Q. S. Zou and X. Y. He, On pressure and velocity boundary conditions for the lattice Boltzmann BGK model, Phys. Fluids, 9(6) (1997), 1591-1598.
[40] M. Rohde, D. Kandhai, J. J. Derksen and H. E. A. van den Akker, Improved bounce-back methods for no-slip walls in lattice-Boltzmann schemes: Theory and simulations, Phys. Rev. E, 67(6) (2003), 066703.
[41] J. H. Masliyah and S. Bhattacharjee, Electrokinetic and Colloid Transport Phenomena, Wiley, New York, 2006.
[42] B. Honig and A. Nicholls, Classical electrostatics in biology and chemistry, Science, 268(5214) (1995), 1144-1149.
[43] R. Qiao and N. R. Aluru, Ion concentrations and velocity profiles in nanochannel electroosmotic flows, J. Chem. Phys., 118(10) (2003), 4692-4701.
[44] W. Zhu, S. J. Singer, Z. Zheng and A. T. Conlisk, Eletro-osmotic flow of a model electrolyte, Phys. Rev. E, 71 (2005), 041501.
[45] M. Wang, J. Liu and S. Y. Chen, Similarity of electro-osmotic flows in nanochannels, Mol. Simulat., 33(3) (2007), 239-244.
[46] Y. H. Qian, D. Dhumieres and P. Lallemand, Lattice BGK models for Navier-Stokes equation, Europhys. Lett., 17 (1992), 479-484.
[47] X. Y. He and L. S. Luo, Theory of the lattice Boltzmann method: From the Boltzmann equation to the lattice Boltzmann equation, Phys. Rev. E, 56(6) (1997), 6811-6817.

[48] S. Y. Chen and G. D. Doolen, Lattice Boltzmann method for fluid flows, Annu. Rev. Fluid Mech., 30 (1998), 329-364.
[49] J. K. Wang, M. Wang and Z. X. Li, Lattice evolution solution for the nonlinear Poisson-Boltzmann equation in confined domains, Commun. Nonlinear Sci. Numer. Simul., 2006. (Published online at doi:10.1016/j.cnsns.2006.06.002).
[50] T. Inamuro, M. Yoshino and F. Ogino, A non-slip boundary condition for lattice Boltzmann simulations, Phys. Fluids, 7(12) (1995), 2928-2930.
[51] D. P. Ziegler, Boundary conditions for lattice Boltzmann simulations, J. Stat. Phys., 71(5/6) (1993), 1171-1177.
[52] D. Yu, R. Mei, W. Shyy and L. S. Luo, Force evaluation in the lattice Boltzmann method involving curved geometry, Phys. Rev. E, 65 (2002), 041203.
[53] P. Lallemand and L. S. Luo, Lattice Boltzmann method for moving boundaries, J. Comput. Phys., 184(2) (2003), 406-421.